Effects of Calcination and Milling Process Conditions for Ceria Slurry on Shallow-Trench-Isolation Chemical–Mechanical Polishing Performance

Japanese Journal of Applied Physics
Vol. 46, No. 12, 2007, pp. 7671–7677

Effects of Calcination and Milling Process Conditions for Ceria Slurry on Shallow-Trench-Isolation Chemical–Mechanical Polishing Performance

Jun-Seok KIM, Hyun-Goo KANG, Manabu KANEMOTO, Ungyu PAIK[1], and Jea-Gun PARK*

Nano-SOI Process Laboratory, Hanyang University, 17 Haengdang-dong, Seoungdong-gu, Seoul 133-791, Korea
[1]*Department of Ceramic Engineering, Hanyang University, 17 Haengdang-dong, Seoungdong-gu, Seoul 133-791, Korea*

(Received September 19, 2006; revised June 29, 2007; accepted August 30, 2007; published online December 6, 2007)

To improve the performance of shallow trench isolation chemical–mechanical polishing (STI-CMP) in terms of the removal selectivity of oxide and nitride films and the formation of surface defects, we investigated the effects of the calcination and milling process conditions during ceria slurry synthesis. We have focused on the effects of particle size distribution, the large-particle size, and the dispersion stability in a ceria slurry. We determined the optimum bead size for milling and appropriate calcination temperatures in order to obtain a reasonable particle distribution, with lower numbers of fine primary particles and large, agglomerated particles, in ceria slurry. This was achieved by reducing the quantity of aggregated particles during milling and two-step calcination process generating higher-density particles. These results can be qualitatively explained by abrasive collisions occurring between the milling beads and the decarbonation of cerium carbonate through diffusion during the manufacturing process used for the ceria slurry. [DOI: 10.1143/JJAP.46.7671]

KEYWORDS: calcination, milling, light point defect, ceria slurry, STI-CMP

1. Introduction

The shallow-trench isolation (STI) process in advanced semiconductor device manufacturing uses chemical–mechanical polishing (CMP) to planarize gap-fill silicon oxide (SiO_2) layers deposited on the front-side surface of a wafer.[1–4] As device dimensions continue to decrease and the leading-edge feature size becomes smaller than 0.1 μm, STI-CMP must be capable of removing a very thin layer of oxide and nitride while leaving a flat surface. In STI-CMP, the selectivity of the removal rates of oxide and nitride films is a critical factor. Moreover, as the oxide and nitride layers become thinner, not only the nitride removal rate but also the numbers of micro-scratches and defects should be controlled more strictly to improve the device characteristics. To improve the selectivity, ceria slurries with anionic surfactants have been used.[3,4,8,11] The anionic surfactant is adsorbed onto the nitride film and acts as a passivation layer, thereby the nitride removal rate is decreased.[13,14,17]

Not only the surfactant characteristics but also the abrasive characteristics are critical issues for STI-CMP ceria slurries. Generally, the film removal rate and the number of surface defects decrease as the abrasive size is reduced, because the mechanical force between the pressed pad and the abrasive particles is weakened.[14] While STI-CMP with smaller abrasive particles leads to a lower number of surface defects, it also leads to other unpredictable effects, such as an increase in the nitride removal rate caused by extra surfactant consumption due to the higher specific surface area of the small particles in the slurry.[17] Therefore, during the synthesis of the ceria slurry, controlling small particles and obtaining a narrow particle size distribution are important factors affecting the oxide-to-nitride removal selectivity. The calcination process is widely used to control the physical characteristics of ceria particles in slurry, including the specific surface area, density, and crystallinity,[11] which greatly affects STI-CMP performance. Specifically, the effect of the two-step calcination reported by our group shows the ability to control the slurry characteristics by calcination.[17] Abrasive particles calcined by two-step calcination are harder and denser, and have a narrower distribution of primary grain size, without large grains that cause microscratches and small primary grains that trigger the agglomeration of colloidal particles, even though the particles have the same grain and secondary particle sizes as these in slurry calcined by one-step calcination. Using these particles, we can improve STI-CMP performance, namely, higher oxide removal rate, higher oxide-to-nitride selectivity, and fewer defects. Moreover, the milling process is used to disperse agglomerates and aggregates and to control the particle size distribution and the shapes of the abrasive particles.[5,6] In particular, the size of the beads used for milling is very important for obtaining abrasive particles in the submicron size range. The applied energy intensity and the rate of stress application in the milling machine also affect the particle size and size distribution.[18,19]

In this study, we investigated the effects of the calcination temperature to study the characteristics of two-step calcination when we manufacture a ceria abrasive from STI-CMP slurry. Moreover, to control the proportions of large and fine particles, which cause microscratches by agglomeration, we investigated the effects of bead size during the milling process after two-step calcination. In addition, we evaluated STI-CMP performance using these slurries.

2. Experimental Procedure

In this study, three types of ceria particles were synthesized from a starting material of high-purity cerium carbonate using the solid-state displacement reaction method. One type of ceria powder was calcined using the one-step calcination method, whereas the other samples were calcined using a two-step calcination method. In the case of one-step calcination, the carbonate precursor was calcined only once at 730 °C for 4 h. In the case of two-step calcination, the ceria particles were obtained through an additional calcination at 550 or 580 °C for 4 h, after initial calcination at 650 or 680 °C, respectively, for 4 h. In addition, between the first and second calcination steps, the ceria particles were crushed with a dry mechanical crusher called an air jet mill. Figures 1(a) and 1(b) show the

*E-mail address: parkjgL@hanyang.ac.kr

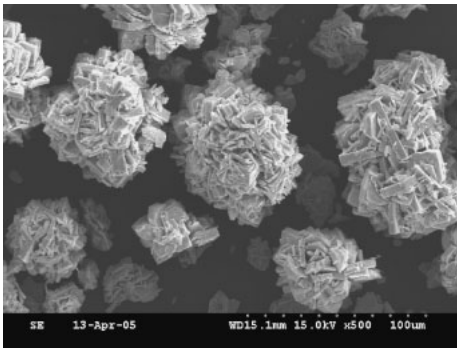

(a)

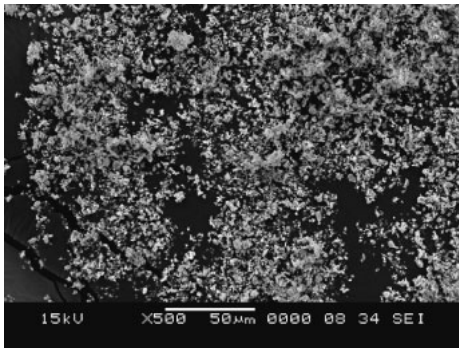

(b)

Fig. 1. SEM images of ceria particles in ceria powder: (a) after first calcination step (680 °C for 4 h) before dry mechanical crushing and (b) after dry mechanical crushing.

ceria particles calcined at 680 °C for 4 h before and after the crushing, respectively. To summarize, the powders calcined in two steps were calcined for a longer period of time and at a lower temperature than those calcined in the conventional manner. In previous studies, we simply explained that the two-step calcination method, in which ceria abrasive particles have an advantage during calcination showing high density and low porosity without abnormal grain growth in manufacturing process of the ceria slurry.[17] In this investigation, however, we focused on not only the two-step calcination process but also the media size during milling process in ceria slurry manufacturing. In addition, we have confirmed the difference in calcination temperature to improve the remaining particles and the nitride film loss while a reasonable oxide removal rate is maintained after CMP. A detailed discussion is provided below.

After the calcination and dry crushing of each powder, the two-step powder calcined at 680 and 580 °C was further crushed by wet mechanical bead milling with different bead sizes of 0.8, 0.4, 0.3, and 0.2 mm, made of ZrO_2, for 3 to 5 h to reduce its secondary particle size to the target size range of 250–300 nm. In contrast, the other two-step powder (calcined at 650 and 550 °C) and the one-step powder were milled using only 0.3 mm beads. The ceria abrasives were then dispersed in deionized water and stabilized by adding 100 ppm of a commercially available dispersant [poly-(methacrylate acid)]. The solid content was controlled at 5 wt % of ceria powder in the ceria suspension. We also optionally added an anionic organic surfactant [poly(acrylic acid)] at different concentrations of up to 0.8 wt %. This surfactant is generally used to control the oxide-to-nitride selectivity with regard to removal rates. Each slurry's pH was adjusted to the range of 6.5–7.5 by adding an alkaline agent. Table I shows a list of the slurry specifications, including the slurry pH values, abrasive sizes, and the experimental conditions used during slurry synthesis.

Table I. Sample preparation conditions.

Item	Calcination temperature (°C)	Bead size (mm)	pH	Secondary particle size (nm)
A	680/580	0.8	6.45	286
B	680/580	0.4	6.55	268
C	680/580	0.3	6.47	275
D	680/580	0.2	6.43	260
E	650/550	0.3	6.60	271
F	730	0.3	6.57	265

The median size of the secondary particles in each slurry was measured by using a Horiba LA910.[10] We obtained images of the ceria particles and measured the primary particle sizes by transmission electron microscopy (TEM), using a JEOL JEM-2010. The specific surface areas of the powders were estimated through Brunauer–Emmett–Teller (BET) method, using a Micromeritics ASAP 2010. The powder densities were measured with a pyconometer, namely, an Micromeritics Accupyc 1330, after the samples were outgassed at 250 °C for 2 h using nitrogen gas to remove physisorbed species from the powder surface.

To investigate the effect the calcination process on STI-CMP performance, CMP evaluation tests were carried out with commercial 8″ wafers covered with plasma-enhanced tetraethylorthosilicate (PETEOS) or low-pressure chemical-vapor deposition (LPCVD) nitride films. The thicknesses of the as-deposited oxide and nitride films were 7000 and 1500 Å, respectively. We polished the films on a Strasbaugh 6EC and carried out *ex situ* conditioning with a diamond dresser before each polishing. We used a Rodel IC1000/Suba IV stacked pad. The polishing pressure, applied as a down force, was 4 psi, equivalent to 27.5 kPa. The relative velocity between the pad and the wafers was 0.539 m/s. The polishing times were 30 s for the oxide films and 90 s for the nitride films. We measured the oxide and nitride thickness variations of the wafers before and after CMP with a Nanometrics NanoSpec 180. The variations in the location and number of light point defects (LPDs) were measured using the stationary beam technology and optional bright field channel of a KLA-Tencor Surfscan SP1. The minimum detection size for LPDs was adjusted to 0.189 μm.

3. Results and Discussion

Figure 2 shows the correlation between the median size (d_{50}) of the secondary particles and the milling time with various bead sizes for the two-step powder calcined at 680 and 580 °C, after dispersion in deionized water. The median size was markedly reduced as the milling time increased. In addition, the smaller bead sizes required significantly shorter milling times than did the largest bead size of 0.8 mm. During the milling process, the secondary particle size is reduced by collision between milling bead and abrasive particle. In addition, the shape and size of fractured particle

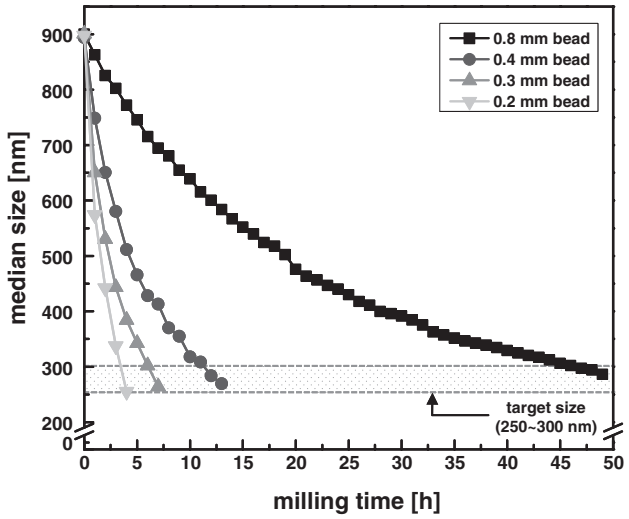

Fig. 2. Change in median size of secondary particles with respect to milling time for two-step powder calcined at 680 and 580 °C.

should be determined by bead size and milling energy, the milling time, and other characteristics of the milling media, if the other parameters of the milling machine are fixed. In particular, the probability of fracture is higher when the frequency of collisions is higher. We assume that if the other parameters except of the bead size are fixed, then the collision frequency per unit volume in the milling machine increases rapidly, as the media size decreases and the media velocity increases.[5] Coarser media have a large spacing with respect to the slurry powder. Thus the collision frequency and contact probability between the beads and the secondary abrasive particles are much lower than those with finer media; accordingly, the secondary particle size is reduced slowly. On the other hand, smaller media have a small spacing with respect to the powder; thus the collision frequency and the probability of fracture are higher, and the secondary particle size is reduced more rapidly. Therefore, as shown by our results, by increasing the milling time, the median size of the secondary abrasives was gradually decreased to within the target range of 250–300 nm even with the largest bead size.

Figure 3 shows the distribution of the primary grain size for the ceria abrasives calcined at 680 and 580 °C, without surfactant addition. The grain sizes were analyzed statistically (30 grains for each set of conditions), and the average

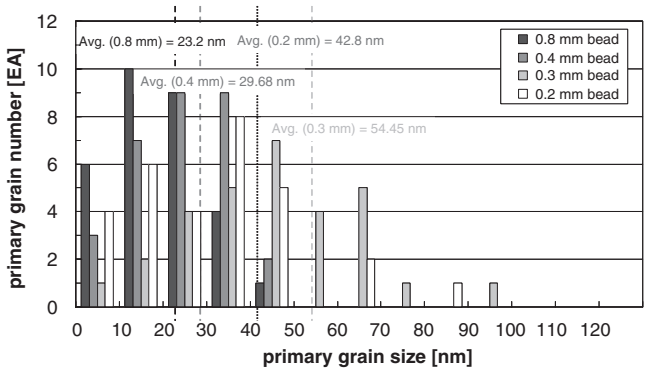

Fig. 3. Particle size distribution of ceria abrasives calcined at 680 and 580 °C.

values were calculated for various bead sizes. Although the secondary abrasive size was fixed in the target range of 250–300 nm, the primary grain size became smaller and had a narrower distribution as the bead size increased. Nevertheless, because the coarsest beads (0.8 mm) have a larger spacing with respect to the powder, the milling time increased as the secondary particle size was slowly reduced, whereas with the smaller bead sizes, the abrasive size was markedly reduced by the beads, which have a smaller spacing with respect to the powder. The beads must not be too small, however, because they must impart sufficient mechanical energy to the particles to cause fracture. In bead milling, for a given volume, the number of balls increases inversely with the cube of the bead radius.[21] The milling rate depends on the number of contact points between the balls and the powder, which in turn depends on the specific surface area of the balls. As shown in Fig. 3, many fine particles (smaller than 10 nm) were produced after milling with the 0.8 and 0.4 mm beads, had small specific surface areas and aggregated around larger particles in order to reduce the total surface energy, thus promoting agglomeration. Such agglomeration reduces the surface potential and stabilizes the slurry system. Hence, fine particles can excessively consume the anionic dispersant and surfactant from the bulk suspension, causing the adsorbed polymer layer on the nitride film to be insufficiently formed. Therefore, in slurry manufacturing, fine particle control is a very important consideration in size reduction induced by bead size control.

Varinot *et al.* previously reported that three milling mechanisms in a stirred bead mill produce different phases in the resulting particle distribution, as shown schematically in Fig. 4.[18] They explained that if the size of the grinding beads is increased or the solid concentration is increased, then fracture becomes dominant with respect to abrasion.[18] Then, under the same conditions, if the applied energy and the rate of stress are constant, the milling mechanism is determined by the hardness of the particles in the slurry suspension. When the particle hardness is high, the local surface stress is relatively lower than that needed to fragment the particle. Abrasion then becomes the dominant mechanism; thus the particles are not fractured but only milled at their edges. None of these different mechanisms occur alone, however, they are always found in combination with one another.

Hence, we consider that the effects of the bead size and the milling time on the size distribution of the secondary abrasive particles are probably directly related. Therefore, the size distribution may be strongly affected by the milling mechanism. In this study, in the case of the slurry milled with 0.2 mm beads, the average particle distribution was shifted to a large size as compared with the slurries milled with larger beads, even though the milling time was shorter. On the other hand, the primary grain particles of the slurry milled with 0.3 mm beads were larger than those in the other slurries, because cleavage was the dominant mechanism reducing the particle size. Both the fine and coarse particles in the slurry were reduced more in size using optimally sized 0.3 mm beads and an appropriate milling time.

We previously reported the physical characteristics of ceria particles with respect to calcination temperature.[11] As

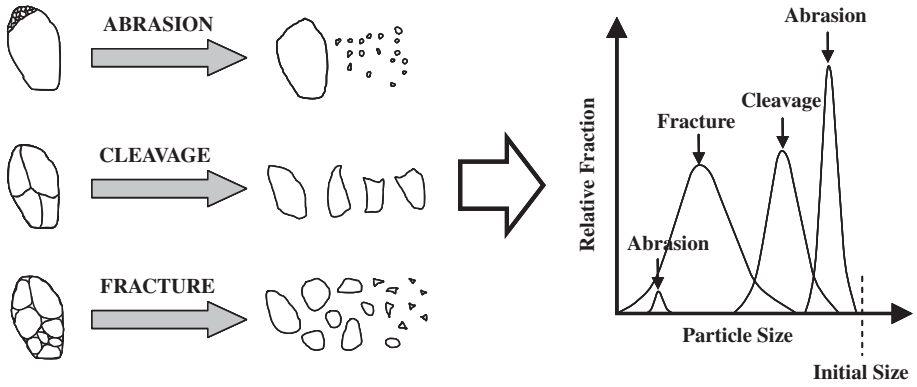

Fig. 4. Schematic illustration of effects of three mechanisms on size distribution of particles after mechanical milling.

the calcination temperature increases, the crystallinity and grain size of ceria particles increase, because of grain growth during calcination as atomic diffusion causes the wetting of the grain boundaries of adjacent grains. These results explain not only the increase in the particle density but also the increasing hardness of the particles. Figure 5 shows high-resolution TEM (HR-TEM) images of abrasive particles milled with 0.3 mm beads after calcination using each of the three processes. As these images indicate, the ceria abrasives had a well-defined morphology and the average size of the primary grains composing the abrasives, as measured from the TEM images, ranged approximately from 30–50 nm. As shown by these images, the primary grains of the ceria abrasives calcined at 650 and 550 °C (a) and 680 and 580 °C (b) were smaller than those of the abrasives calcined only at 730 °C (c). Kosynkin *et al.* previously reported that the oxidation reaction of the cerium carbonate precursor to synthesis the ceria particles, consisting of decarbonation and crystal growth, is not always completed at a specific temperature and that both the decarbonation and crystal growth are more efficient in different temperature ranges.[20] In fact, at a lower calcination temperature, the efficiency of the decarbonation of cerium carbonate is high, while the crystal growth rate is low. At a higher temperature, however, the relationship is reversed i.e., slow decarbonation and rapid crystal growth. Therefore, during calcination at a low temperature, the density increases rapidly while the grain size increases slowly, since most of the energy is used not for crystal growth but for decarbonation. Thus, by controlling decarbonation and crystal growth, it is possible to obtain dense, hard, uniform-sized particles, with uniform-sized primary grains. During calcination at a high temperature of 730 °C in the one-step process, on the other hand, the primary grain size increases rapidly, since the grains combine with each other to stabilize themselves by reducing the total surface energy. As a consequence, the one-step slurry had primary grains larger than 100 nm, which were larger than those of the two-step calcined slurries. However, its density was lower, because the core of the large primary grains reacts more slowly than the outer part of the particles and thus cannot be calcined completely.

Additionally, in case of the ceria abrasives calcined at 680 and 580 °C had the lowest number of primary grains consisting of fine particles less than 10 nm in size. By the two-step calcination, it would be possible to generate dense

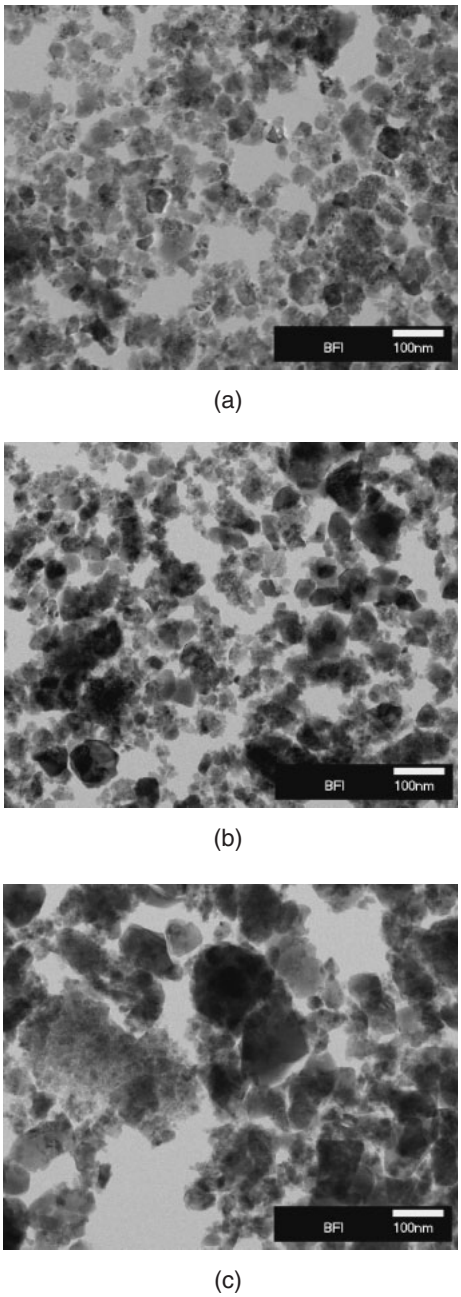

Fig. 5. TEM images showing ceria particles after milling with 0.3 mm beads: calcined at (a) 650 and 550, (b) 680 and 580, and (c) 730 °C.

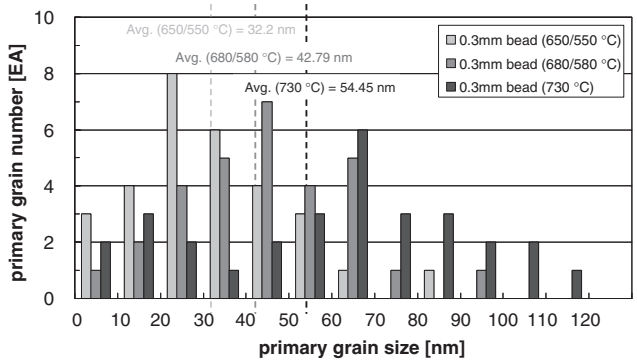

Fig. 6. Particle size distribution of ceria abrasives milled with 0.3 mm beads.

particles with a higher degree of synthesis than one-step calcined abrasive, has lower agglomerated large particle and fine primary grains.[17] Even though the ceria abrasives were synthesized by the same two-step calcination (650/550 °C and 680/580 °C), there is a difference in the proportion of fine particles. Furthermore, with the ceria abrasives calcined at 730 °C, it is more produced the large secondary particle by agglomeration of many number of fine primary grains less than 10 nm by calcinations process with high temperature. It is thought that two-step calcined abrasive particle, which was calcined at a low temperature, had less large grains than one-step calcined abrasive. Hence, the fine particles produced by collision between milling beads and abrasive particle during milling process, which was made the broader distribution of particle size.

Figure 6 shows the distribution of the primary grain sizes of the ceria abrasives for all three slurries after milling with 0.3 mm beads, before dispersant addition. The primary grain size of the ceria particles is reduced through the mechanical milling process, although initially all the particles are the same size. The primary grain size had a slightly broader distribution for the one-step slurry, and the proportion of large particles was also higher than that for the two-step slurries. Hence, we concluded that the crystallinity of the one-step sample was higher than that of the other samples; the particles in this case were broken through edge grinding during the milling process caused by the abrasion mechanism explained above. Regarding the primary grain size of the two-step slurry calcined at low temperatures (650 and 550 °C), however, the primary particles have a lower crystallinity and are easily broken by the dominant fracture mechanism, because these particles have a lower hardness than those calcined at higher temperatures. On the other hand, for the medium-sized abrasives calcined at 680 and 580 °C, the cleavage mechanism is dominant, because of the appropriate surface stress and mechanical force between the milling media and the abrasive polycrystalline ceria particles. Therefore, the ceria abrasive calcined at 680 and 580 °C has fewer fine particles smaller than 10 nm in size. By controlling the calcination temperature and the bead size of the milling process, we can obtain ceria particles having fewer fine particles smaller than 10 nm in size.

In STI-CMP, the removal rates of the oxide and nitride films, the selectivity, uniformity, and LPD formation are generally affected by several factors, including the abrasive

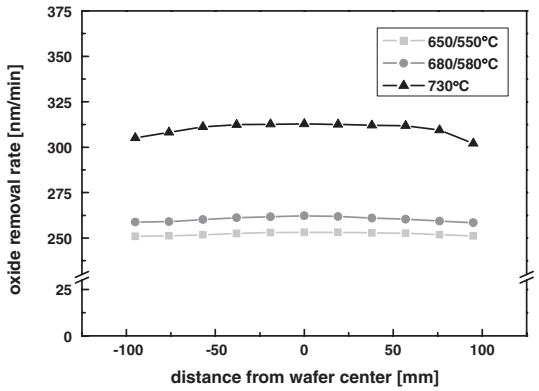

(a)

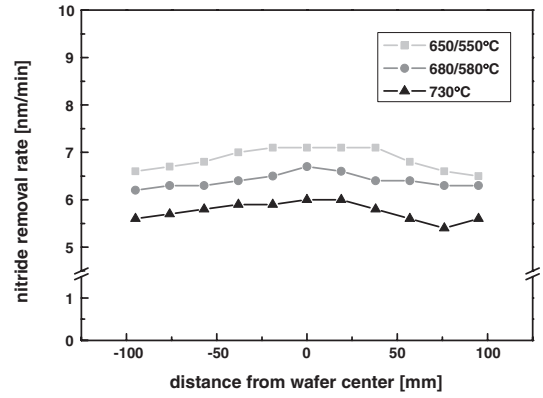

(b)

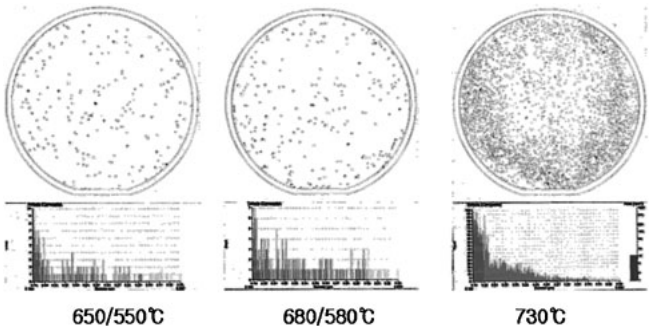

(c)

Fig. 7. Results of CMP tests: (a) oxide removal rate, (b) nitride removal rate, and (c) maps of the remaining particles on oxide film after CMP.

Table II. Summary of CMP test results.

Item	Oxide removal rate (Å/min)	Nitride removal rate (Å/min)	Selectivity	Particle count on oxide film (larger than 0.189 μm)
C	2522	68	37.1	209
E	2534	65	39.0	242
F	3102	58	53.5	2220

morphology, grain size, secondary particle size, and particle size distribution. We previously reported the effects of agglomerated particles on LPD formation, removal rate, and removal selectivity.[8,9] As the number of agglomerated particles increases, the number of LPDs increases. Figure 7 and Table II show the results of our CMP tests, including the

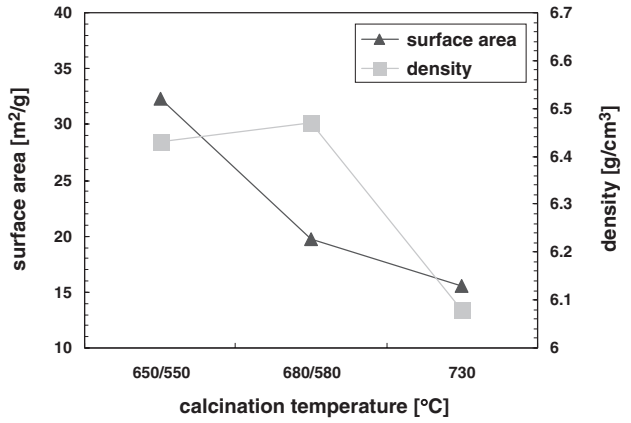

Fig. 8. Densities and specific surface areas for different calcination temperatures.

removal rates of the oxide and nitride films and the LPD counts on the oxide surfaces. The oxide removal rate usually depends on the primary grain size, as shown in Fig. 6. As the grain size increases, the oxide removal rate also increases, whereas the nitride removal rate remains almost the constant when the concentration of the additive is above a critical value.[13–15] We previously reported a removal mechanism for an oxide film with a ceria slurry.[12] In this mechanism, the kinematical energy of the abrasives is the dominant factor in oxide polishing; that is, the abrasive size, polishing pressure, relative velocity between the table and the head, and other factors affect the removal rate of oxide film.[12,14] The nitride removal rate of the slurry calcined in one-step process was lower than that of the other samples, and the two-step slurry showed a slightly higher nitride removal rate; specifically the slurry calcined at 650 and 550 °C showed the highest removal rate. We previously reported the relationship between the molecular weight of PAA and the oxide-to-nitride selectivity in STI-CMP.[22] PAA is adsorbed on both the oxide and nitride films, but it is more strongly adsorbed onto the nitride film; thus, a denser passivation layer is formed as the molecular weight of PAA increases. That is the nitride removal rate was affected by the amount of PAA adsorbed onto film. The result of nitride removal rate can be explained by this mechanism. As shown in Fig. 8, which is discussed below in detail, with an increase in calcination temperature, the surface area of the slurry decreases. Moreover, with an increase in surface area, the particles consume more PAA molecules. Thus, the particles can excessively consume the surfactant from the bulk suspension, causing the adsorbed polymer layer on the nitride film to be insufficiently formed.[16] Consequently, the nitride removal rate increases with the proportion of surface area, resulting in poor oxide-to-nitride removal selectivity. Therefore, as the calcination temperature increases, the removal selectivity increases. The number of LPDs, however, increased drastically for the slurry calcined at 730 °C, as shown in Fig. 7(c). As noted above, we previously reported the effects of agglomerated particles on the removal rates of oxide and nitride films.[9] These agglomerated particles cause many LPDs after polishing.[8] In this study, the slurry calcined at 730 °C had not only more agglomerated particles but also more primary grains larger than 100 nm in size, as shown in Fig. 5(c). It is consider that these agglomerated particles and large grains cause the formation of many LPDs. As discussed above, with an increase in calcination temperature, the oxide-to-nitride removal selectivity increases, and the removal rate of nitride film decreases, however, the number of LPDs increases.

Figure 8 shows the specific surface area and the density of the slurry particles after drying the synthesized powder. The densities of the two-step samples were higher than that of the one-step sample, and specific surface area showed the same tendency. This means that the ceria particles of the two-step samples were denser and harder (less porous), because of the higher degree of synthesis, than those of the one-step sample. However, in our experiment, the oxide removal rate was affected more by primary grain size than by hardness of the particles, as shown in Figs. 6 and 7(a). Moreover, the nitride removal rates were different, that the selectivity for the one-step sample was better than that for the two-step samples. As noted above, however, it is considered that the agglomerated particles and large grains cause the formation of many LPDs. Therefore, to improve the STI-CMP performance, ceria slurries with large proportions of both fine and agglomerated large particles should be carefully controlled using an optimum bead size during milling.

4. Conclusions

We investigated the effects of calcination and milling process conditions during ceria slurry synthesis on film removal and the formation of LPDs. During a continuous mechanical milling process after calcination, fine particles were formed with a longer milling time using coarser beads. The slurries with many fine particles excessively consumed the surfactant in the bulk suspension and formed agglomerates because of the particles' large specific surface area. In our experiments, we found that the optimum bead size was 0.3 mm with a two-step process of calcination at 680 and 580 °C. This approach generated a appropriate particle distribution in the ceria slurry, with lower levels of fine primary grains and large agglomerated particles, because during the milling process, the abrasive particles were broken predominantly through a cleavage mechanism. Hence, the nitride removal rate was different value in this case, meaning better selectivity with a larger primary grain size and more agglomerated particles for slurries calcined in one step than for slurries calcined in two steps. The agglomerated particles and large grains, however, caused the formation of many LPDs. Therefore, to improve STI-CMP performance, ceria slurries with large proportions of both fine and agglomerated large particles should be carefully controlled by using an optimum bead size during milling.

Acknowledgement

This study was supported by the Korea Ministry of Science and Technology through the National Research Laboratory (NRL) program. We thank SUMCO Corp. and Hynix Semiconductor, Inc. for helping us with our experiments. We are also indebted to Mr. Jin-Hyung Park, Mr. Kyung-Woong Park, Mr. Hyuk-Yul Choi, Mr. Byoung-Seok Lee, and Mr. Keum-Seok Park for assisting us in performing the experiments.

1) S. Wolf: *Silicon Processing for the VLSI Era: Process Integration* (Lattice Press, Sunset Beach, CA, 1990) Vol. 4, Chap. 13, p. 24.
2) H. S. Park, K. B. Kim, C. K. Hong, U. I. Chung, and M. Y. K. Lee: Jpn. J. Appl. Phys. **37** (1998) 5849.
3) K. Hirai, H. Ohtsuki, T. Ashizawa, and Y. Kurata: Hitachi Chemical Tech. Rep. **35** (2000) 17.
4) H. Nojo, M. Kodera, and R. Nakata: IEDM Tech. Dig., 1996, p. 349.
5) J. S. Reed: *Principles of Ceramics Processing* (Wiley-Interscience, New York, 1995) 2nd ed., Chap. 17, p. 323.
6) T. Chartier, S. Souchard, J. F. Baumard, and H. Vesteghem: J. Eur. Ceram. Soc. **16** (1996) 1283.
7) J. R. McLaughlin: Ceram. Ind. **149** (1999) No. 12, p. 34.
8) H. G. Kang, T. Katoh, D. H. Kim, U. Paik, and J. G. Park: Jpn. J. Appl. Phys. **44** (2005) L238.
9) D. H. Kim, H. G. Kang, S. K. Kim, U. Paik, and J. G. Park: Jpn. J. Appl. Phys. **44** (2005) 7770.
10) V. A. Hackley and J. Texter: in *Ultrasonic and Dielectric Characterization Techniques for Suspended Particulates*, ed. V. A. Hackley and U. Paik (American Ceramic Society, Westerville, OH, 1998) p. 191.
11) S. K. Kim, P. W. Yoon, U. Paik, T. Katoh, and J. G. Park: Jpn. J. Appl. Phys. **43** (2004) 7427.
12) T. Katoh, H. G. Kang, U. Paik, and J. G. Park: Jpn. J. Appl. Phys. **42** (2003) 1150.
13) Y. Tateyama, T. Hirano, T. Ono, N. Miyashita, and T. Yoda: Proc. Int. Symp. Chemical Mechanical Planarization IV, Phoenix, 2000, p. 297.
14) J. G. Park, T. Katoh, W. M. Lee, H. Jeon, and U. Paik: Jpn. J. Appl. Phys. **42** (2003) 5420.
15) H. G. Kang, M. Y. Lee, H. S. Park, U. Paik, and J. G. Park: Jpn. J. Appl. Phys. **44** (2005) 4752.
16) M. Itano, T. Kezuka, M. Ishii, T. Unemoto, M. Kubo, and T. Ohmi: J. Electrochem. Soc. **142** (1995) 971.
17) D. H. Kim, H. G. Kang, S. K. Kim, U. Paik, and J. G. Park: Jpn. J. Appl. Phys. **45** (2006) 4893.
18) C. Varinot, S. Hiltgun, M.-N. Pons, and J. Dodds: Chem. Eng. Sci. **52** (1997) 3605.
19) M. Gao and E. Forssberg: Powder Technol. **84** (1995) 101.
20) V. D. Kosynkin, A. A. Arzgatkina, E. N. Ivanov, M. G. Chtoutsa, A. I. Grabko, A. V. Kardapolov, and N. A. Sysina: J. Alloys Compd. **303–304** (2000) 421.
21) M. N. Rahaman: *Ceramic Processing and Sintering* (Marcel Dekker, New York, 1995) Chap. 2, p. 42.
22) C. W. Cho, S. K. Kim, U. Paik, J. G. Park, and W. M. Sigmund: J. Mater. Res. **21** (2006) 473.